

Understanding and Preventing Lubrication Failure at the Carbon Atomic Steps

Wenmeng Yan, Fakhrul H. Bhuiyan, Chuan Tang, Liang Wei, Yilong Jiang, Seokhoon Jang, Yangqin Liu, Jiang Wu, Wen Wang, Yang Wang, Ashlie Martini, Linmao Qian,* Seong H. Kim,* and Lei Chen*

Two-dimensional (2D) lamellar materials are normally capable of rendering super-low friction, wear protection, and adhesion reduction in nanoscale due to their ultralow shear strength between two basal plane surfaces. However, high friction at step edges prevents the 2D materials from achieving super-low friction in macroscale applications and eventually leads to failure of lubrication performance. Here, taking graphene as an example, the authors report that not all step edges are detrimental. The armchair (AC) step edges are found to have only a minor topographic effect on friction, while the zigzag (ZZ) edges cause friction two orders of magnitude larger than the basal plane. The AC step edge is less reactive and thus more durable. However, the ZZ structure prevails when step edges are produced mechanically, for example, through mechanical exfoliation or grinding of graphite. The authors found a way to make the high-friction ZZ edge superlubricious by reconstructing the (6,6) hexagon structure to the (5,7) azulene-like structure through thermal annealing in an inert gas environment. This will facilitate the realization of graphene-based superlubricity over a wide range of industrial applications in which avoiding the involvement of step edges is difficult.

1. Introduction

Friction and wear are the primary modes of mechanical energy dissipation in engineering systems operating with mechanical moving parts, which account for nearly one-fifth of the world's energy consumption.^[1] Two-dimensional (2D) lamellar

materials with a few atomic layers or even one single layer can provide super-low interfacial friction. Thus, 2D materials can be a good candidate for mitigation of parasitic energy loss due to friction. Among various 2D materials, graphene is of great interest because it is known to have excellent chemical inertness and mechanical strength. Its super-low friction originates from the atomically flat and crystallographically incommensurate contact of its inert basal plane with counter surfaces.

Although such a structural superlubricity can readily be achieved at the nanoscale where sliding is limited to the basal plane region. [5] It is usually unobtainable in larger-scale applications, especially when the sliding distance is larger than the size of the graphene domains. Friction at a single-layer graphene step edge is $>10^2$ times larger than that on the basal plane. [6] The graphene edges are also vulnerable to

wear, which is another challenging issue to maintain durable and long lifetime super-low friction.^[7] One strategy to circumvent these challenges could be using graphene nanosheets in combination with nanoscale particles, such as nanodiamond particles^[8] and silica nanospheres.^[9] It was proposed that graphene-wrapped nanoscrolls could be formed around nanoparticles, which could prevent graphene edges from adversely affecting friction and wear.

W. Yan, C. Tang, L. Wei, Y. Jiang, Y. Liu, W. Wang, Y. Wang, L. Qian, L. Chen Tribology Research Institute
State Key Laboratory of Traction Power
School of Mechanical Engineering
Southwest Jiaotong University
610031 Chengdu, China
E-mail: linmao@swjtu.edu.cn; chenlei@swjtu.edu.cn

The ORCID identification number(s) for the author(s) of this article can be found under https://doi.org/10.1002/smll.202301515

© 2023 The Authors. Small published by Wiley-VCH GmbH. This is an open access article under the terms of the Creative Commons Attribution-NonCommercial-NoDerivs License, which permits use and distribution in any medium, provided the original work is properly cited, the use is non-commercial and no modifications or adaptations are made.

DOI: 10.1002/smll.202301515

F. H. Bhuiyan, A. Martini Department of Mechanical Engineering University of California Merced, CA 95343, USA

S. Jang, S. H. Kim

Department of Chemical Engineering and Materials Research Institute Pennsylvania State University

University Park, PA 16802, USA E-mail: shkim@engr.psu.edu

J. Wu

Institute of Fundamental and Frontier Sciences and State Key Laboratory of Electronic Thin Film and Integrated Devices

University of Electronic Science and Technology of China 610054 Chengdu, China



Regardless of the length scale, stable superlubricity relies on maintaining incommensurate sliding contact.^[3] The presence of step edges in the sliding contact area inevitably leads to the loss of this structural super-low friction.^[10,11] Thus, it is important to better understand mechanisms causing high friction at graphene step edges to facilitate engineering design. Such knowledge can be used to mitigate or prevent lubrication failure at the step edge.

2. Results and Discussion

Graphene has a honeycomb lattice and the termination of the periodic lattice is formed along two crystallographic directions, which are known as zigzag (ZZ) and armchair (AC) edges.[12] These two are either 30° or 90° to each other. Although they may appear identical in topographic images, they can be distinguished with the D-band at ≈1350 cm⁻¹ in Raman spectroscopy. [13] The D-mode is active at the AC edge due to the double resonance process, but it is inactive at the ZZ edge since the scattered momentum is not aligned with the adjacent Dirac cones, as illustrated in the inset in **Figure 1**A.^[14,15] A 90° corner of a graphene layer on a mechanically exfoliated graphite basal plane (Figure 1A) was characterized with micro-Raman spectroscopy. The step height was ≈160 nm (Figure S1A,B, Supporting Information). The Dband signal was strong at one side of the corner and undetectable at the other side (Figure 1B). The full spectrum collected at one location of each edge (Figure 1C) confirmed that the upper edge has AC structure and the lower one has ZZ structure.

The friction behavior at another 90° corner with AC and ZZ steps was characterized with atomic force microscopy (AFM) with a Si probe (nominal tip diameter d = 4-6 nm). The AFM topography in Figure 1D shows that the step height is ≈ 0.34 nm, indicating a single-layer graphene edge. The lateral force image, obtained simultaneously with the topographic image at an applied load of 15 nN in ambient air (45 \pm 5% relative humidity, 23 \pm 2 °C), exhibited significantly higher friction at the steps as compared with the basal plane. In Figure 1D, it is noted that the upper step of the 90° corner had significantly lower friction than the lower one. To quantify friction at each step, the trace and retrace lateral force signals are plotted (Figure 1F). The line profiles show that the step-up resistive force at the lower edge is almost one order of magnitude larger than that at the upper one. Based on the previous study[16,17] and the relative abundance of these two distinct friction patterns (Figure S2, Supporting Information), the high friction edge is confidently identified as the ZZ step. Then, the low friction one must be the AC step. A similar difference in friction was observed at thick ZZ and AC steps (Figure S1C, Supporting Information) defined in Figure 1A–C.

The friction force measured on the basal plane was around 0.05 ± 0.02 nN at the applied normal force of 15 nN, which gave a coefficient of friction (COF) of ≈ 0.003 (adhesion force was below 1 nN). This COF value is consistent with the superlubricity reported in the literature. At the AC step, friction had no significant change, except a small topographic perturbation. In contrast, the ZZ step showed friction ≈ 100 times larger than the basal plane, resulting in a COF of ≈ 0.3 . This means that the ZZ step edge is the main cause for the loss of superlubricity, while the AC step has no detrimental effect.

In addition to the difference between the magnitudes of the step-up resistive force, the local variance of friction is quite different between the ZZ and AC edges. During the step-down process at the ZZ edge (BB' profile in red in Figure 1F), friction increased initially (negative lateral force in the retrace), then decreased (positive lateral force), and finally increased again before it fully returned to the basal plane value. A similar pattern was also observed in Ref.[16,17], and was identified as the characteristic behavior of exposed graphene steps that were mostly the ZZ edge.[18] The complex step-down friction behavior was due to the combined effects of chemical (hydrogen bonding across the interface) and topographic (strain) contributions. [16] During the step-up process, the effects of chemical and topographic contributions led to a large resistive force. At the AC step edge (AA' profile in blue in Figure 1F), the AFM lateral signals due to friction during the step-up and step-down processes were almost identical. This implied that the chemical (interfacial bonding) effect was negligible at the AC edge and that topographic effects (resistive during step-up and assistive during step-down) were dominant. The buried step edge also exhibited the topographic effect only.[16] This comparison suggests that, in terms of friction, the AC step exposed at the graphite surface behaves similarly to the step buried under another layer of graphene.

The relative magnitudes of the ZZ and AC edge friction at single-layer steps can be compared by measuring the AFM lateral signals at corners where two edges meet (Figure 1G). Representative topographic and friction responses measured at single-layer graphene corners with various edge angles are shown in Figure S3 (Supporting Information). Figure 1H displays the maximum peak forces for the step-up resistive component as a function of the step angle with respect to the reference ZZ edge. The stepup resistive force is about ten times smaller at the AC edge than at the ZZ edge. During the step-down at the AC edge, the resistive component is often below the detection limit (Figure S4A, Supporting Information) and the assistive force due to topography change is similar to the step-up resistive force in magnitude (Figure S4B, Supporting Information). The intermediate values at edges slightly off the crystallographic orientation (periodic angular interval of 60°) could be due to the copresence of ZZ and AC sites with varying distributions in the contact area. [19] In addition, the magnitude of the friction force difference between the ZZ and AC edges did not vary with the scan angle with respect to the edge orientation (Figure S5, Supporting Information). The friction at the ZZ edge increased approximately linearly with increasing the applied load, while the AC edges showed a very weak dependence on the load (Figure S6, Supporting Information).

What causes such a large difference in friction between these edges? The electronic structures of the ZZ and AC edges are different^[20]; so, one may ask if it plays a dominant role. **Figure 2A**,B shows the low-magnification topographic and friction images of a 30° graphene corner with ZZ and AC edges, respectively. The high-magnification conductive AFM (c-AFM) images of the ZZ and AC edge regions (marked as I and II in Figure 2A) are shown in Figure 2B,C, respectively. The c-AFM scan direction was parallel to the edge direction in Figure 2A. In both c-AFM images, the periodic pattern with a=0.246 nm corresponds to the graphene lattice. The ZZ edge had irregular or serrated structures (Figure 2C), while the AC edge was relatively straight (Figure 2D). The ZZ edge has spin-polarized electrons accumulated near the Fermi energy which form a flat band. This localized edge state is responsible for the large change in electrical



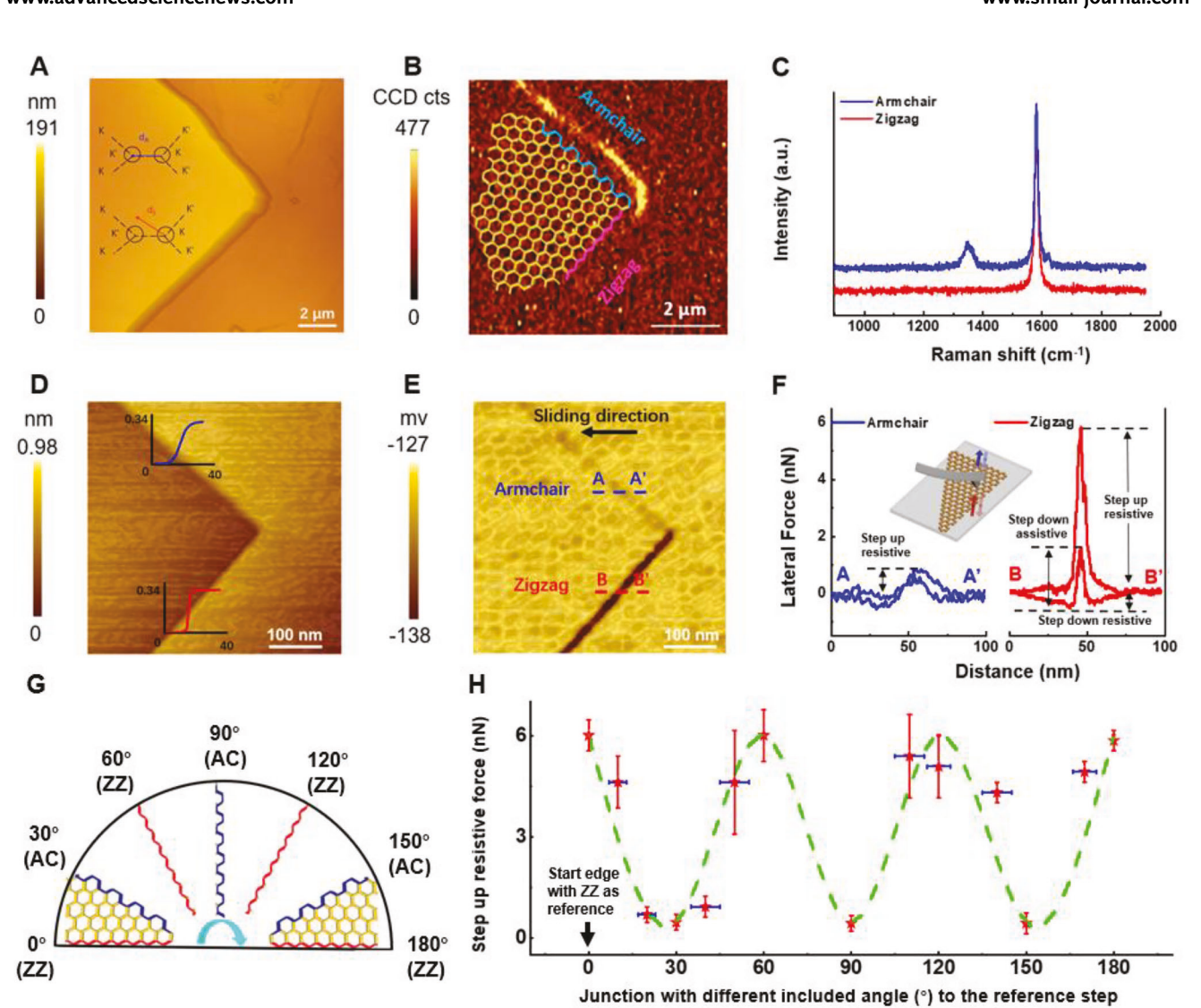


Figure 1. Different friction responses at the AC and ZZ graphene step edges, respectively. A) Topography of a 90° junction with ≈150 nm thickness. The height profile and friction behavior for the upper and bottom steps are shown in Figure S1 (Supporting Information). Insets schematically show that the double resonance process of ZZ edge is forbidden since the exchanged momentum by scattering from ZZ (d_Z) deviates from the adjacent K and K' Dirac cones; in contrast, the exchanged momentum from AC can satisfy the intervalley scattering process. B) Raman image of the D band intensity at the horizontal laser polarization. The inset schematic shows the atomic structure of the 90° junction connecting the AC-ZZ step. C) Raman spectra taken at the AC (upper blue spectrum) and ZZ (bottom red spectrum) steps. D) Topography of another 90° junction connecting the armchair-zigzag step. Inset profiles show the monolayer thickness. E) Friction images of the monolayer step edge in a scan area of 500 × 500 nm. F) Representative lateral forces measured at AC and ZZ graphene steps with an applied load of 15 nN. G) The schematic image shows the edge structure of the junction with different included angles (°). H) Maximum peak forces for the step-up resistive component as a function of edge angle with respect to a reference ZZ edge (calculated from Figure S3, Supporting Information). The step-down resistive and step-down assistive components can be seen in Figure S4 (Supporting Information).

conductance across the ZZ step (Figure 2E). In contrast, the conductance change across the AC step is relatively small and occurs gradually over several lattice units (Figure 2F). This is due to the delocalization of electronic states at the AC step.^[24]

Such a difference in electronic charge distribution could affect the interfacial adhesion force. [25,26] The pull-off force needed to separate the Si AFM probe from the surface (Figure 2G) was measured during the line scan across the ZZ and AC edges. Figure 2H shows that the adhesion force at the ZZ edge (\approx 2.45 nN) is larger than that at the AC edge (\approx 1.45 nN). How-

ever, the magnitude difference in adhesion force of the ZZ and AC edges is much smaller than that in friction force (Figure 1G). Moreover, the friction force measured at the graphene step edge on the graphite basal plane does not necessarily correlate with the adhesion force measured at the same location. ^[27] Thus, the origin of the friction difference could be something else.

We have investigated if the large difference in friction between the ZZ and AC edges could be due to their chemical reactivities, using reactive molecular dynamics (MD) simulations. [16] The Si probe with a native oxide layer was modeled with a semicircular

and-conditions) on Wiley Online Library for rules of use; OA articles are governed by the applicable Creative Commons License

www.advancedsciencenews.com



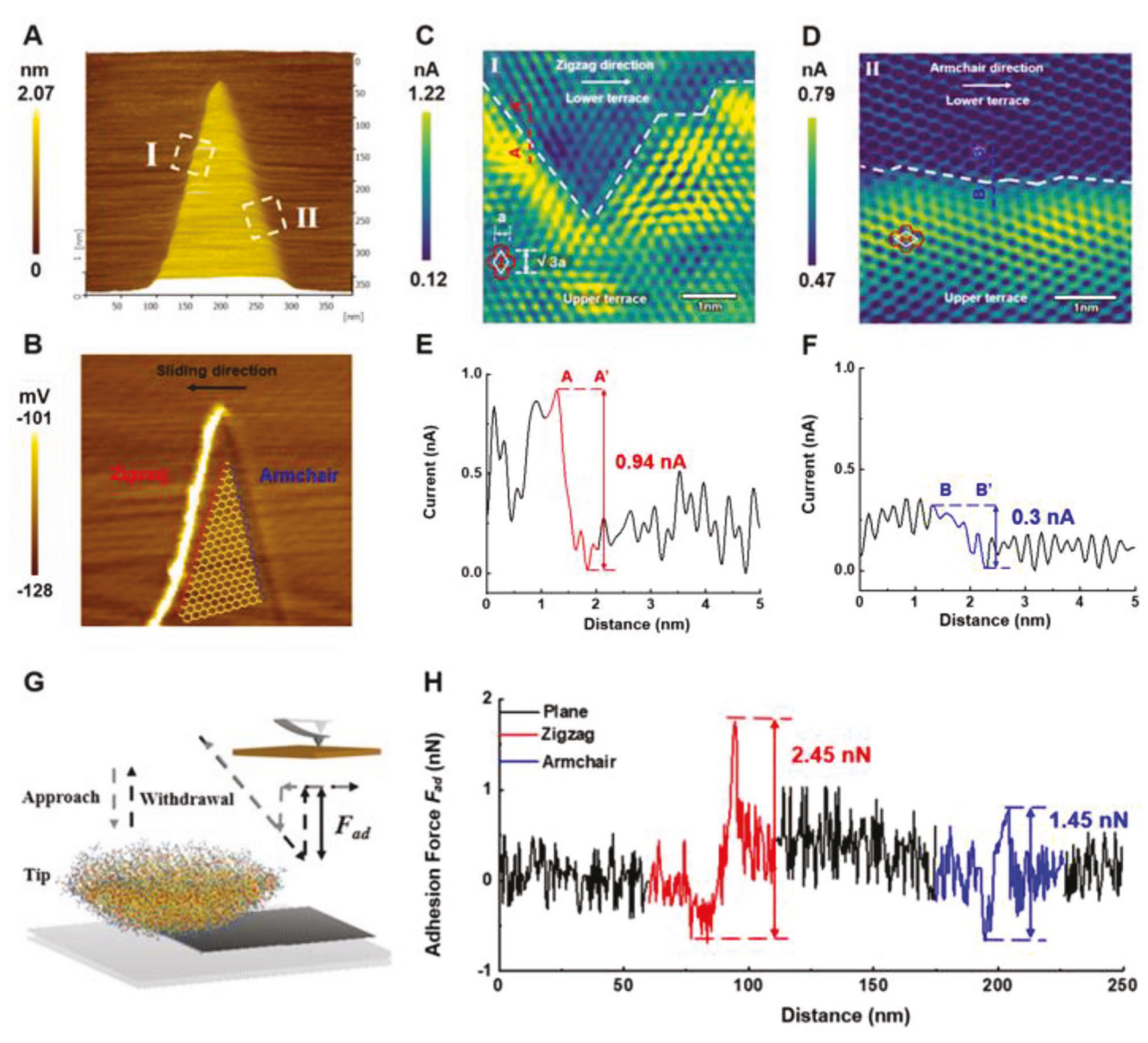


Figure 2. The atomic lattice images and adhesion force of ZZ and AC edges, respectively. A) Topography and B) friction image of graphene step edges with an included angle of 30° . The schematic diagram in (B) shows the atomic structure of ZZ and AC. C,D) Atomic lattice images of the ZZ and AC step edges marked with boxes in (A) scanned with c-AFM (imaging conditions: Vs = 800 mV, imaging area $V = 5 \times 5$ nm²). E,F) Currented measured across (E) ZZ and (F) AC step edges. G) Schematic diagram of adhesion test. H) Adhesion force measured at the ZZ and AC step edges.

disc of amorphous silica (**Figure 3A**). The outermost surface of the probe was passivated with H atoms. Considering the serrated shape of the ZZ edge, we created two steps with the ZZ structure with different angles in a small simulation box. To one end of the ZZ edge, the AC edge was connected at a 90° angle. The carbon atoms at the graphene edge were terminated with –H and –OH alternately (Figure 3A). The simulations showed that, during the step-up process at a compressive force of 10 nN, friction at the AC edge was \approx 4 nN (Figure 3B), which was lower than friction at the corner where the AC and ZZ edges met (\approx 6.5 nN; Figure 3C) and at the ZZ edge \approx 6.5 nN; Figure 3D). Although the magnitude of the simulated friction did not match quantitatively with the AFM data, the qualitative trends were consistent with the experimental observations.

The reactive MD simulations showed that interfacial bonding between the probe and the edge is significantly larger at the ZZ edge as compared with the AC edge. When a silica surface was slid over the AC edge, the number of transient covalent bonds between the probe surface and the carbon atom was relatively small and they readily dissociated as the probe moved onto the upper terrace (Figure 3E). At the corner between the two edges, slightly more transient covalent bonds were formed and they were easily dissociated (Figure 3F). In contrast, at the ZZ edge, many covalent bonds were formed across the sliding interface, and they did not dissociate readily (Figure 3G). In the simulation, these strong covalent bonds at the ZZ edge even pulled the graphene edge along the scan direction as the probe moved onto the upper terrace (Movie S1, Supporting Information). These results are quite

16136829, 0, Downloaded from https://onlinelibrary.wiley.com/doi/10.1002/smll.202301515 by Pennsylvania State University, Wiley Online Library on [31.07/2023]. See the Terms and Conditions (https://onlinelibrary.wiley.com/doi/10.1002/smll.202301515 by Pennsylvania State University, Wiley Online Library on [31.07/2023]. See the Terms and Conditions

nditions) on Wiley Online Library for rules of use; OA articles are governed by the applicable Creative Commons License

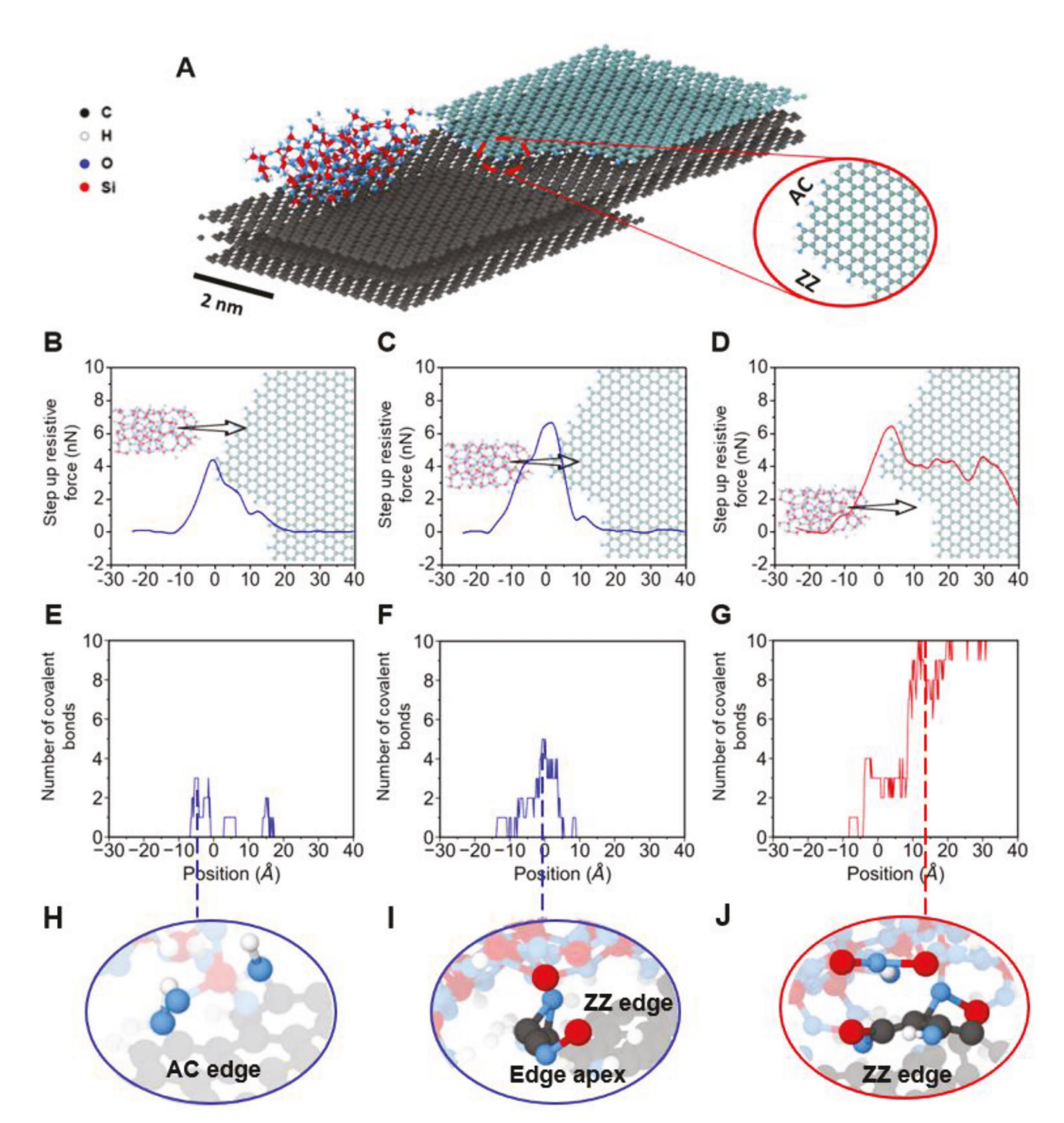


Figure 3. MD simulations of friction and covalent bond formation between the amorphous silica probe and the graphene edge terminated with H/OH alternatively. A) The simulated system had a silica probe and a graphite slab with both AC and ZZ edges. The black, white, blue, and red atoms represent C, H, O, and Si, respectively. The C atoms on the upper terrace were colored differently for visual illustration. In three simulations, the tip was slid over the AC edge (left), corner where the two edges met (middle), and the ZZ edge (right). B-G) Peak friction measured (B-D) and number of Si-O-C covalent bonds formed (E-G) during the sliding. H-J) Close-up snapshots of representative interfacial bonds taken when the number of bonds between the tip and the edge was maximum.

consistent with the fact that the ZZ edge is more chemically reactive than the AC edge.^[28,29] The fact that more and stronger Si-O-C covalent bonds are formed at the ZZ edges than on the AC edges (Figure 3H–J) could explain why friction is much larger at the ZZ edge than the AC edge.

This chemical reactivity difference at ZZ and AC edges may also explain the difference in topography recorded in contactmode AFM. In the AFM images of the steps in the insets of Figure 1D and Figures S3 and S5 (Supporting Information), the slope of the cross-section profile line at the ZZ edges is

nditions) on Wiley Online Library for rules of use; OA articles are governed by the applicable Creative Commons License

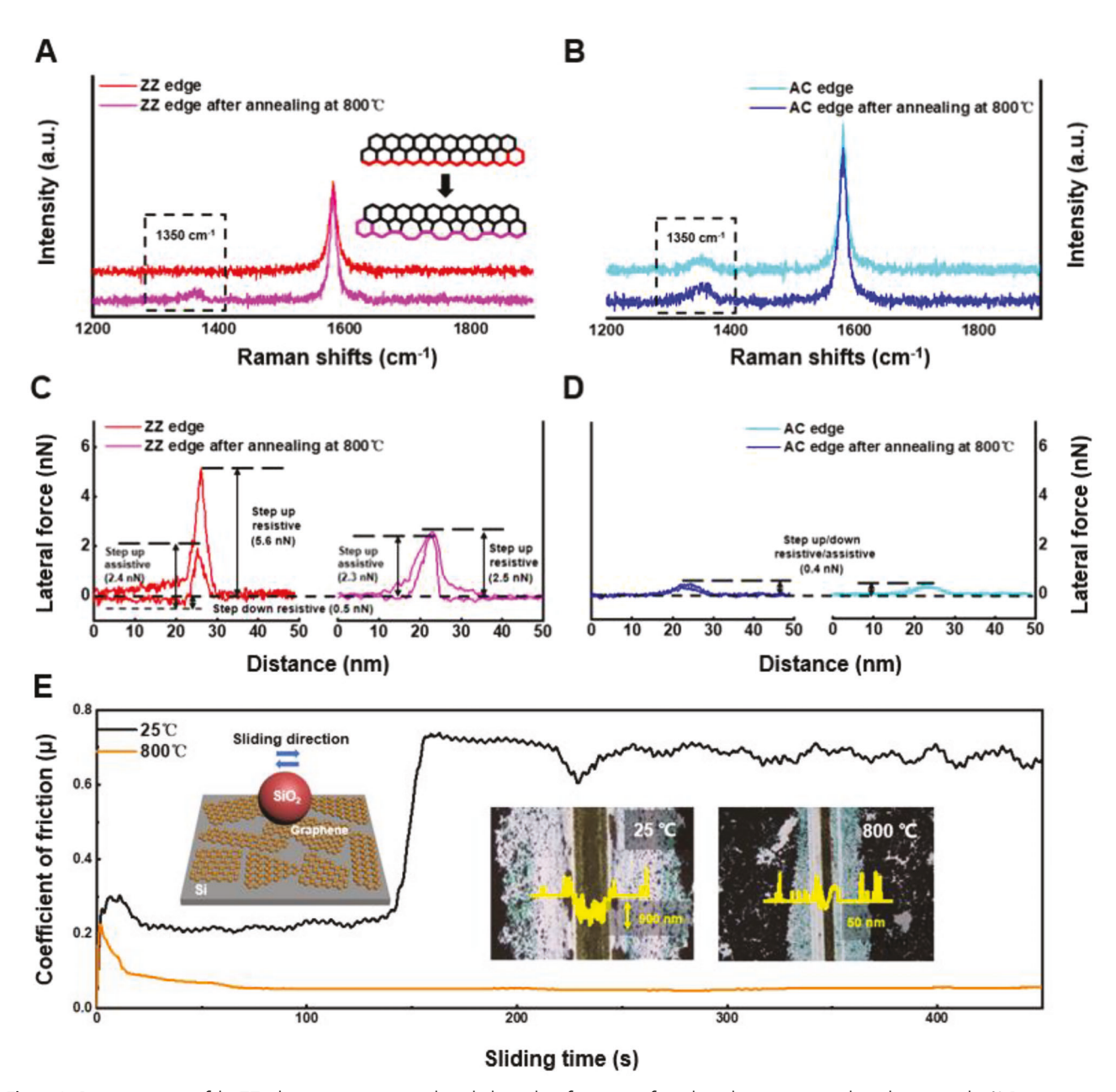


Figure 4. Reconstruction of the ZZ edge structure to tune the tribological performance of graphene layer at nanoscale and macroscale. A) Raman spectra of the ZZ step edge before and after annealing at 800 °C in argon. Inset schematically shows the reconstruction of the ZZ edge structure from the pristine (6,6) structure to the azulene-like pentagon-heptagon alternating structure. B) Raman spectra of the AC step edge before and after annealing at 800 °C. C,D) The nanoscale lateral forces at the ZZ and AC step edges before and after annealing at 800 °C measured using a Si AFM probe. The applied load was 15 nN. E) Macroscale friction measured with a silica ball (radius = \approx 3 mm) sliding on a Si wafer with graphene nanosheets without and with annealing at 800 °C in argon. The applied load was 1N and the sliding speed was 2.4 mm s⁻¹. The inset in the left side is a schematic rendition of the ball-on-flat tribotesting. The insets in the right side are optical images comparing the wear scars and the corresponding cross-section profiles of the pristine and annealed graphene films on silicon substrates.

 $78.3\pm2.6^{\circ}$, which is larger than the slope at the AC edges (72.5 \pm 0.6°). It is possible that, at the AC edge, the tip ascends smoothly and gradually over the atomic step. But, at the ZZ edge, the tip motion could be locally pinned because the transient Si–O–C bonds do not dissociate readily. Thus, for the AFM probe to ascend the ZZ step, the dissociation of interfacial bonds must occur

concertedly, which increases friction and affects the measured topography.

This finding suggests that if graphene nanosheets were produced predominantly with AC edges, it might resolve the lubrication failure issue in macroscale applications. Although graphene nanoribbons are produced mostly with the AC termination in





www.small-journal.com

bottom-up fabrication,^[30,31] it is difficult to scale up for mass production. When graphene flakes or powders are produced by mechanical exfoliation of graphene layers from crystalline graphite, the ZZ edges are produced predominantly (Figure S2, Supporting Information). This is because the propagation of C–C bond ruptures is energetically more favorable along the ZZ direction than the AC direction.^[32] The pristine ZZ step consists of sixmembered rings (hereafter called (6,6) structure), but when it is annealed thermally, a structural reconstruction occurs forming the alternative patterns of the azulene-like pentagon–heptagon (5,7) structures.^[33] The reconstructed (5,7) structure is more stable than the pristine (6,6)-ZZ structure.^[33–35] Thus, the reconstructed (5,7)-ZZ edge is expected to be less reactive than the pristine (6,6)-ZZ edge.

To test this hypothesis, we have annealed the graphite surface with graphene step edges at 800 °C in inert argon gas. The Raman spectra measured at a ZZ step (Figure 4A) exhibited the D peak at 1350 cm⁻¹ after annealing at 800 °C in argon, indicating the rearrangement of ZZ structure to the (5,7) structure, which satisfies double resonance and hence activates the D-mode. [36] In comparison, the Raman spectrum at an AC step did not change before and after annealing (Figure 4B). Interestingly, the maximum friction force (step-up resistive force) at the annealed ZZ step measured using a nanoscale Si probe decreased by ≈50% upon annealing (Figure 4C), while the friction at the AC step had no change with annealing (Figure 4D). The ZZ step reconstruction can possibly produce two structures—(5,7) and AC.[28,34,37,38] Among these two, the (5,7) reconstruction is believed to be more likely. It requires a smaller displacement of edge atoms as compared with the reconstruction to the AC structure. Also, the friction at the anneal ZZ edge (Figure 4C) exhibited a much larger topographic effect than that at the AC edge (Figure 4D). Based on these reports and observations, the reconstructed structure is most likely to be the (5,7)-ZZ structure, rather than the AC struc-

Lastly, we have tested if the annealing effect observed in the nanoscale AFM experiment is manifested in the macroscale lubrication. The graphene nanosheets were deposited on a silicon wafer and friction was measured with a SiO2 ball (radius = \approx 3 mm) in room air before and after annealing at 800 °C (inset in Figure 4E). The unannealed graphene film showed a rapid failure, increasing friction coefficient from ≈ 0.2 initially to ≈0.7 after about 150 cycles of reciprocating sliding with a wear depth similar to that observed with a bare silicon wafer (Figure S7, Supporting Information). In contrast, the annealed graphene layer exhibited a gradual decrease of friction coefficient to ≈ 0.08 for a significantly prolonged period (Figure 4E) and a reduction of wear depth by $\approx 95\%$ (insets in Figure 4E). The wear debris on the tested SiO2 spheres was analyzed (Figure S8, Supporting Information). The wear debris was found to be significantly less after sliding on the annealed coating as compared with the case of sliding on the unannealed coating. Raman analysis showed that the debris on the sphere surface was graphene flakes, which probably contributed to the overall lubricity.[39] If the annealing temperature was high enough to drive off adsorbed water but not sufficient to induce reconstruction, then the lubrication efficacy did not improve (Figure S9, Supporting Information).

3. Conclusion

In summary, the AFM measurements of friction at the corners of single-layer graphene steps with various edge angles revealed that the step edge friction is highly dependent on the edge structure. The pristine ZZ structure gives about two orders of magnitude larger friction than the basal plane surface, while the AC structure exhibits only a marginal increase. The large friction at the ZZ edge could be ascribed to the high chemical reactivity of the (6,6)-ZZ structure. Thermal annealing induces the reconstruction of the ZZ edge from the (6,6) structure to the more stable (5,7) structure, which leads to a significant reduction in friction and a substantial improvement in lubrication performance in the macroscale tribotesting. This finding could facilitate the engineering design of graphene step edges that could enable high reliability and a long lifetime of graphene superlubricity in all length scales.

Supporting Information

Supporting Information is available from the Wiley Online Library or from the author.

Acknowledgements

W.M.Y., C.T., L.W., Y.L.J., Y.Q.L., L.M.Q., and L.C. acknowledges the support from the National Natural Science Foundation of China (grant Nos. 51875486, 52122507, 52235004, 51991317). S.H.J. and S.H.K. acknowledge the support from the National Science Foundation of the USA (grant No. CMMI-1912199). This work was also supported by the Sichuan Science and Technology Program (grant No. 2023NSFSC1988) and the Fundamental Research Funds for the Central Universities (grant No. 2682021ZTPY095).

Conflict of Interest

The authors declare no conflict of interest.

Author Contributions

L.C., S.H.K., and L.M.Q. conceived the concept. W.M.Y., C.T., L.W., and S.J. conducted the experiments and characterizations. L.C., W.M.Y., T.C., Y.Q.L., and Y.L.J. analyzed the obtained data. F.H.B. and A.M. did the MD simulations. W.M.Y., F.H.B., A.M., S.H.K., and L.C. co-wrote the manuscript. J.W., W.W., and Y.W. provided expertise. L.C. supervised the research as a project leader and coordinated the preparation of the manuscript. All the authors have given approval to the final version of the manuscript. All the authors discussed the results and commented on the manuscript.

Data Availability Statement

The data that support the findings of this study are available from the corresponding author upon reasonable request.

Keywords

atomic step chemistry, carbon materials, super-low friction

Received: February 20, 2023 Revised: April 9, 2023 Published online:



- [1] K. Holmberg, A. Erdemir, Friction 2017, 5, 263.
- [2] O. Hod, E. Meyer, Q. S. Zheng, M. Urbakh, Nature 2018, 563, 485
- [3] M. Dienwiebel, G. S. Verhoeven, N. Pradeep, J. W. M. Frenken, J. A. Heimberg, H. W. Zandbergen, Phys. Rev. Lett. 2004, 92, 126101.
- [4] C. Lee, X. Wei, J. W. Kysar, J. Hone, Science 2008, 321, 385.
- [5] Y. Shi, X. Yang, B. Liu, H. Dong, Q. Zheng, Nanotechnology 2016, 27, 325701.
- [6] C. Qu, K. Wang, J. Wang, Y. Gongyang, R. W. Carpick, M. Urbakh, Q. Zheng, Phys. Rev. Lett. 2020, 125, 126102.
- [7] Y. Qi, J. Liu, J. Zhang, Y. Dong, Q. Li, ACS Appl. Mater. Interfaces 2017, 9, 1099.
- [8] D. Berman, S. A. Deshmukh, S. K. Sankaranarayanan, A. Erdemir, A. V. Sumant, *Science* 2015, 348, 1118.
- [9] S. Liu, H. Wang, Q. Xu, T. Ma, G. Yu, C. Zhang, D. Geng, Z. Yu, S. Zhang, W. Wang, Y. Hu, H. Wang, J. Luo, Nat. Commun. 2017, 8, 14029
- [10] K. Wang, C. Qu, J. Wang, B. Quan, Q. Zheng, Phys. Rev. Lett. 2020, 125, 026101.
- [11] S. Li, Q. Li, R. W. Carpick, P. Gumbsch, X. Liu, X. Ding, J. Sun, J. Li, Nature 2016, 539, 541.
- [12] L. G. Cancado, M. A. Pimenta, B. R. Neves, M. S. Dantas, A. Jorio, Phys. Rev. Lett. 2004, 93, 247401.
- [13] J. Kim, N. Lee, Y. H. Min, S. Noh, N. K. Kim, S. Jung, M. Joo, Y. Yamada, ACS Omega. 2018, 3, 17789.
- [14] B. Krauss, P. N. Incze, V. Skakalova, L. P. Biro, K. Klitzing, J. H. Smet, Nano Lett. 2010, 10, 4544.
- [15] A. K. Gupta, T. J. Russin, H. R. Gutierrez, P. C. Eklund, ACS Nano. 2009, 3, 45.
- [16] L. Chen, Z. Chen, X. Tang, W. Yan, Z. Zhou, L. Qian, S. H. Kim, Carbon 2019. 154, 67.
- [17] Z. Chen, A. Khajeh, A. Martini, S. H. Kim, Sci. Adv. 2019, 5, eaaw0513.
- [18] N. Wohner, P. Lam, K. Sattler, Carbon 2014, 67, 721.
- [19] Y. Kobayashi, K. Fukui, T. Enoki, K. Kusakabe, Y. Kaburagi, Phys. Rev. B 2005, 71, 193406.
- [20] K. A. Ritter, J. W. Lyding, Nat. Mater. 2009, 8, 235.

- [21] Y. Niimi, T. Matsui, H. Kambara, K. Tagami, M. Tsukada, H. Fukuyama, Appl. Surf. Sci. 2005, 241, 43.
- [22] S. Fujii, M. Ziatdinov, M. Ohtsuka, K. Kusakabe, M. Kiguchia, T. Enoki, Faraday Discuss. **2014**, *173*, 173.
- [23] X. Jia, M. Hofmann, V. Meunier, J. C. Delgado, J. M. Romo-Herrera, H. Son, Y. P. Heieh, A. Reina, J. Kong, M. Terrones, M. S. Dresselhaus, *Science* 2009, 323, 1701.
- [24] S. E. Stein, R. L. Brown, J. Am. Chem. Soc. 2002, 109, 3721.
- [25] K. Nakada, M. Fujita, G. Dresselhaus, M. S. Dresselhaus, *Phys. Rev. B* 1996, 54, 17954.
- [26] M. Wolloch, G. Levita, P. Restuccia, M. C. Righi, Phys. Rev. Lett. 2018, 121, 026804.
- [27] Z. Chen, M. R. Vazirisereshk, A. Khajeh, A. Martini, S. H. Kim, J. Phys. Chem. Lett. 2019, 10, 6455.
- [28] S. Okada, Phys. Rev. B 2008, 77, 041408.
- [29] D. E. Jiang, B. G. Sumpter, S. Dai, J. Chem. Phys. 2007, 126, 134701.
- [30] R. M. Jacobberger, B. Kiraly, M. Fortin-Deschenes, P. L. Levesque, K. M. Mcelhinny, G. J. Brady, R. R. Delgado, S. S. Roy, A. Mannix, M. G. Lagally, P. G. Evans, P. Desjardins, R. Martel, M. C. Hersam, N. P. Guisinger, M. S. Arnold, *Nat. Commun.* 2015, 6, 8006.
- [31] J. M. Cai, P. Ruffieux, R. Jaafar, M. Bieri, T. Braun, S. Blankenburg, M. Muoth, A. P. Seitsonen, M. Saleh, X. L. Feng, K. Müllen, R. Fasel, *Nature* 2010, 466, 470.
- [32] W. X. Zhang, Tarek, R., Cemal. Basaran, Int. J. Damage Mech. 2017, 26, 447.
- [33] K. He, A. W. Robertson, Y. Fan, C. S. Allen, Y.-C. Lin, K. Suenaga, A. I. Kirkland, J. H. Warner, ACS Nano. 2015, 9, 4786.
- [34] Y. N. Xu, D. Zhan, L. Liu, H. Suo, Z. X. Shen, ACS Nano. 2011, 5, 147.
- [35] P. Koskinen, S. Malola, H. Häkkinen, Phys. Rev. Lett. 2008, 101, 115502.
- [36] S. Malola, H. Hkkinen, P. Koskinen, Eur. Phys. J. D. 2009, 52, 71.
- [37] B. Song, G. F. Schneider, Q. Xu, G. Pandraud, C. Dekker, H. Zandbergen, Nano Lett. 2011, 11, 2247.
- [38] B. Westenfelder, J. C. Meyer, J. Biskupek, S. Kurasch, F. Scholz, C. E. Krill, U. Kaiser, Nano Lett. 2011, 11, 5123.
- [39] P. Wu, X. Li, C. Zhang, X. Chen, S. Lin, H. Sun, C.-T. Lin, H. Zhu, J. Luo, ACS Appl. Mater. Interfaces 2017, 9, 21554.